ELSEVIER

Biophysical Chemistry 90 (2001) 75–87

Biophysical Chemistry

www.elsevier.nl/locate/bpc

Interactions of cyclic AMP and its dibutyryl analogue with model membrane: X-ray diffraction and Raman spectroscopic study using cubic liquid–crystalline phases of monoolein

Valdemaras Razumas[a,*], Gediminas Niaura[a], Zita Talaikytė[a], Adomas Vagonis[a], Tommy Nylander[b]

[a] *Institute of Biochemistry, Mokslininkų 12, LT-2600 Vilnius, Lithuania*
[b] *Department of Physical Chemistry 1, Center for Chemistry and Chemical Engineering, P.O. Box 124, S-221 00 Lund, Sweden*

Received 1 August 2000; received in revised form 31 October 2000; accepted 19 December 2000

Abstract

Interactions of adenosine 3′:5′-cyclic monophosphate (cAMP) and its dibutyryl analogue, N^6,2′-*O*-dibutyryladenosine 3′:5′-cyclic monophosphate (dbcAMP), with a lipid bilayer were studied by small-angle X-ray diffraction (SAXD) and Raman spectroscopy. The cubic *Pn3m* phase of monoolein (MO) served as a bilayer-based model system. SAXD measurements have indicated that incorporation of approximately 3 wt.% cAMP leaves the phase parameters practically unaltered, whereas the same content of dbcAMP induces the intercubic *Pn3m* → *Ia3d* transition. By applying the concepts of lipid shape parameter and infinite periodic minimal surface to these MO phases, we have suggested that, as opposed to cAMP, dbcAMP associates with the MO bilayer. This conclusion has been supported by the different effects of phase matrix on the Raman shifts of the adenine and phosphate vibrational modes of these two nucleotides. Moreover, Raman spectra have indicated that dbcAMP inserts into the bilayer through the butyryladenine group, positioning dbcAMP preferentially at the polar/apolar interface.

Keywords: Cyclic AMP; Dibutyryl cyclic AMP; Monoolein bilayer; Bicontinuous cubic phase; X-Ray diffraction; Raman spectroscopy

* Corresponding author. Tel.: +370-2-729144; fax: +370-2-729196.
E-mail address: vrazumas@bchi.lt (V. Razumas).

0301-4622/01/$ - see front matter
PII: S0301-4622(01)00133-8

1. Introduction

The discovery of adenosine 3′:5′-cyclic monophosphate (cAMP; Fig. 1) by Sutherland and co-workers (see, e.g. Sutherland and Rall [1]) was the key step in the formation of the current concept of hormone signaling through secondary messengers. Despite the fact that many other secondary messengers have been discovered since then, cAMP, up to now, remains the focus of attention of numerous investigations. One such research area is related to the cellular site of cAMP generation.

It is well known that cAMP is formed by a family of membrane enzymes, adenylyl cyclases, and, hence, it might be speculated that the hormone-stimulated buildup of cAMP concentration at the membrane/cytosol interface affects the properties of biomembrane lipid phase. Actually, this hypothesis is supported by experimental results. For example, when employing oocytes [2] and erythrocytes [3] as model systems, it has been demonstrated that cAMP changes the fluidity of membranes. Thus, in the study of human erythrocytes by Raman spectroscopy, Li et al. [3] have shown that, at cAMP concentrations higher than 10^{-6} M, the conformational order of the acyl chains of lipids decreases slightly, whereas the mobility of the zwitter-ionic head-groups of phospholipids increases.

It is hardly surprising that the spectroscopic effects observed by Li et al. [3] were rather poorly defined (particularly for the head-group and C–H stretching vibration modes). Because it is very polar, cAMP penetrates the cell membrane only in very small quantities. This fact is well-known from numerous experiments of the exogeneous application of cAMP to the cells. Thus, to mimic a hormonal message across the plasma membrane of the intact cell, it is necessary to use high doses

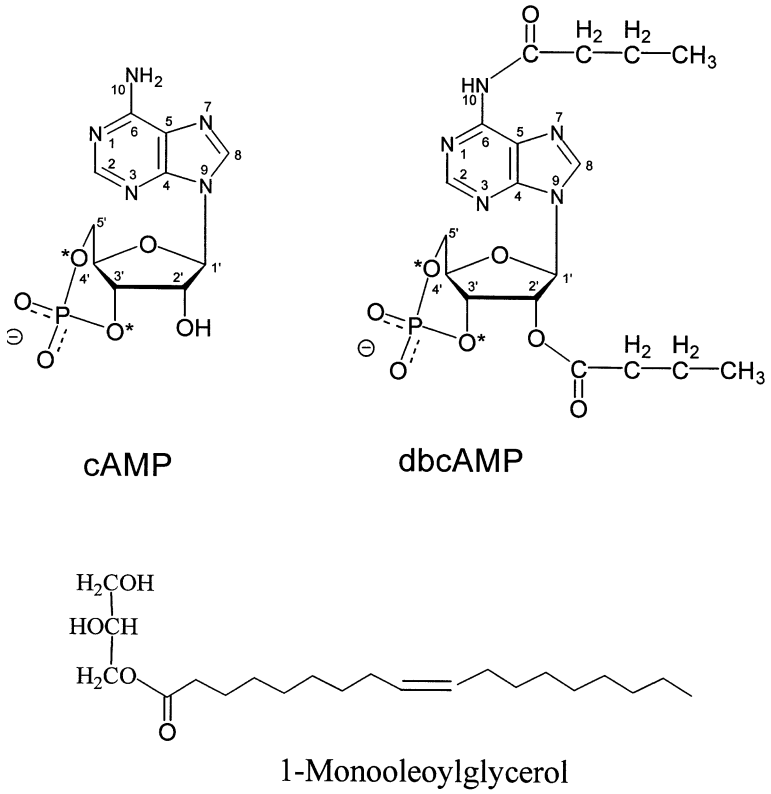

Fig. 1. Molecular structures of adenosine 3′:5′-cyclic monophosphate (cAMP), N^6,2′-*O*-dibutyryladenosine 3′:5′-cyclic monophosphate (dbcAMP), and 1-monooleoylglycerol.

of cAMP, exceeding by several orders of magnitude the physiological levels (approx. 10^{-8}–10^{-6} M). For this reason, in hope of increasing the permeability across the membrane, Posternak, Sutherland and Henion [4] have introduced the first acyl derivatives of cAMP. From among all of the substances synthesized, N^6,2′-*O*-dibutyryladenosine 3′:5′-cyclic monophosphate (dbcAMP; Fig. 1) showed the highest physiological activity.

Although hundreds of cAMP derivatives have been synthesized and investigated since the pioneering work by Posternak et al. [4], the dibutyryl analogue of cAMP is still largely used in biological experiments. However, it was not the intention of our paper to discuss and expand the research area of the hormonal action of cyclic nucleotides. Rather, using cAMP and dbcAMP as representative examples of the natural and synthetic cellular messengers, in the present report, we have introduced the reversed ('water-in-oil' type) bicontinuous cubic phases of aqueous monoolein (MO; Fig. 1 shows the structure of 1-monooleoylglycerol which constitutes the greater part of MO) as lipid bilayer-based systems for the model investigation of biomembrane-cyclic nucleotide interactions. It is important to note that there are compelling evidences of the occurrence of the bicontinuous cubic structures ('cubic membranes') in many cell types and their organelles [5]. Therefore, for the present purposes, the choice of cubic phases looks quite well-founded, although it should be remembered that the cellular cubic membranes and the lipid cubic phases differ in a number of features (e.g. different scales of periodicity, mechanisms of stabilization presumably also differ, etc.).

At 25°C and with increasing water content, 1-monooleoylglycerol forms two reversed bicontinuous phases of cubic symmetry [6–8]: (i) the phase of space group type *Ia3d* (19–38 wt.% of water); and (ii) the phase of space group type *Pn3m* (37–42 wt.% of water; at higher water content, this cubic phase coexists with bulk water). According to our earlier investigation [8], the presence of diglycerides and polyunsaturated monoglycerides in the commercial preparation of MO (see Section 2) shifts the phase boundaries towards lower water content by up to 6 wt.%.

On the basis of investigations performed to date (see, e.g. [6,10–14]), the reversed cubic phases of aqueous 1-monooleoylglycerol and MO can be visualized in terms of a curved continuous lipid bilayer, which subdivides three-dimensional space into two disjointed continuous water channels. Moreover, for these cubic mesophases, the center of the lipid bilayer is expected to lie on an infinite periodic minimal surface (IPMS) of hyperbolic shape. Specifically, the *Ia3d* and *Pn3m* cubic phases can be represented by the 'gyroid'- (G) and 'diamond'-type (D) IPMS, respectively (Fig. 2). All IPMS including the G- and D-type surfaces have zero mean curvature and non-positive Gaussian curvature at all points, whereas parallel surfaces a distance $\pm l$ from IPMS have non-zero mean curvatures.

Among other things, there is also practical interest in the cubic phases of lipids. For example, since the *Pn3m* cubic phase of 1-monooleoylglycerol or MO is stable in the presence of excess water, this structure has already found use in the development of drug delivery systems [15,16], protein crystallization matrices [17,18], complex bioelectrodes [19,20] and enzyme-based biosensors [21,22]. For the same stability reasons, in the present study, we chose the MO *Pn3m* cubic phase containing 39 wt.% of H_2O (or D_2O) as a reference system. Furthermore, this phase was modified by the entrapment of approximately 3 wt.% of cAMP or dbcAMP. To evaluate the MO bilayer–cyclic nucleotide interactions, the reference and cAMP (or dbcAMP)-containing systems were analyzed by two techniques: small angle X-ray diffraction (SAXD) and Raman scattering spectroscopy.

2. Experimental

The mixture of mono- and diglycerides (approx. 25:1 w/w), denoted as monoolein (MO), was kindly provided by Danissco Ingredients (Brabrand, Denmark) with the following acyl chain composition (batch TS-ED 173): 90 wt.% oleic acid; 5 wt.% linoleic acid; 2.7 wt.% stearic acid; 1 wt.% palmitic acid; 0.3 wt.% linolenic acid; and 1 wt.% other fatty acids. The same batch of MO was used in all experiments. Sodium salt of adenosine 3′:5′-cyclic monophosphate

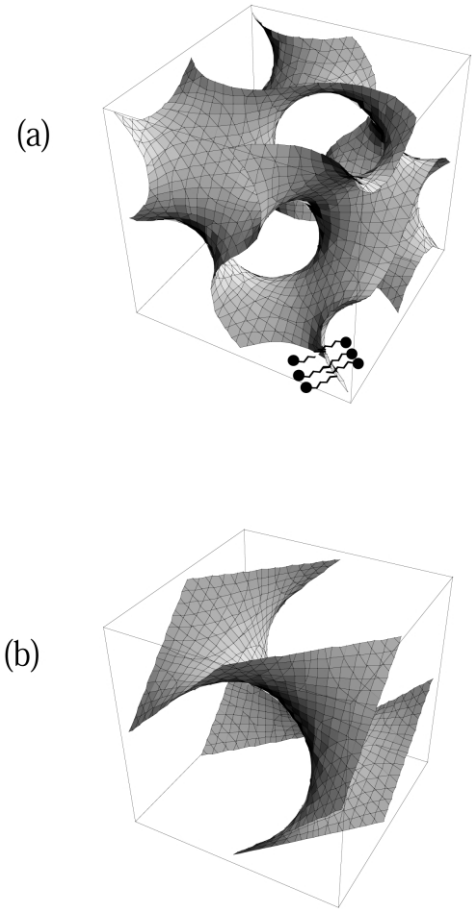

Fig. 2. The infinite periodic minimal surfaces (IPMS) are the structural bases of the reversed bicontinuous cubic phases. The unit cells of (a) the G-type surface which forms the mid-plane of a lipid bilayer of the *Ia3d* cubic phase, and (b) the D-type surface which forms the bilayer mid-plane of the *Pn3m* cubic phase. The lipid bilayer is indicated at the bottom of (a).

(cAMP; purity ca. 98%, Reanal, Hungary), sodium salt of N^6,2′-*O*-dibutyryladenosine 3′:5′-cyclic monophosphate (dbcAMP; purity ca. 97%, Sigma, USA) and deuterium oxide (D_2O; 99.9 at.% of D, Isotech, USA) were used as received. The water was distilled and passed through a Milli-Q water purification system (Millipore S.A., Molsheim, France).

Samples were prepared by weighing appropriate amounts of MO into 6-mm (i.d.) glass ampoules, melting MO at 40°C, and then adding appropriate volumes of pure solvents or of the cAMP or dbcAMP solutions in H_2O or D_2O. The ampoules were immediately flame-sealed and the samples were then centrifuged for 1 h at $3000 \times g$ and 25°C before storing them in the dark at 20°C for at least 2 weeks.

Small-angle X-ray diffraction (SAXD) studies were performed at 20°C using a Kratky compact small angle system equipped with a position sensitive detector OED 50M (MBraun, Graz, Austria) containing 1024 channels of width 53.1 μm. Cu K_α nickel-filtered radiation ($\lambda = 1.542$ Å) was provided by a Seifert ID 3000 X-ray generator (Rich. Seifert & Co, Ahrensburg, Germany), operating at 50 kV and 40 mA. Diffraction data were collected over 2–3 h at a sample-to-detector distance of 277 mm. Temperature control within 0.1°C was achieved by using a Peltier element.

Raman spectra were recorded by a computer-controlled DFS-24 spectrometer (Leningradskoje Optiko-Mekhanitcheskoje Ob'jedinenije, St. Petersburg, Russian Federation) with samples in a glass ampoule using 90° scattering geometry. An argon ion laser LGN-503 (Lvov, Ukraine) was used for the excitation of the samples at 514.5 nm. The laser plasma lines were attenuated by means of an interference filter. Spectra were recorded at 2 cm^{-1} resolution and with laser power of approximately 50 mW. The Raman scattering light was analyzed by a f/5.3 double monochromator with 1200 lines/mm gratings, and detected by a water cooled (to approx. 10°C) photomultiplier and a photon counting system. Spectroscopic experiments were performed at 20°C. The overlapping Raman bands were deconvoluted into the sum of Gaussian and Lorentzian shapes. Positions, bandwidths and amplitudes were varied until good agreement was achieved between actual and simulated spectra (correlation coefficients were no less than 0.999).

3. Results and discussion

3.1. Small-angle X-ray diffraction study

Small-angle X-ray diffraction (SAXD) provides information on the long-range organization of the

liquid–crystalline phases of lipids and, therefore, this technique was applied to establish possible effects of cAMP and dbcAMP (as well as of D_2O) on the essential structural features of the cubic mesophase(s) of MO.

Table 1 presents the results of SAXD measurements for the pseudobinary and pseudoternary systems (recall that monooleoylglycerol comprises only 86 wt.% of the MO preparation). The indexing of the diffraction data was performed as shown in Fig. 3 by a plot of d_{hkl} vs. $(h^2 + k^2 + l^2)^{-1/2}$, where d_{hkl} is the spacing of Bragg reflections, and

Table 1
X-Ray diffraction data of the cubic phase samples

Cubic phase composition	d_{hkl} (Å)	hkl	Space group	a_o (Å)[a]
MO/H_2O (61:39 wt.%)	68.8	110		
	56.4	111		
	48.7	200		
	39.9	211	*Pn3m*	97.0 ± 0.9
	34.6	220		
	32.5	221, 300		
MO/D_2O (60.9:39.1 wt.%)	68.9	110		
	55.5	111		
	47.9	200		
	39.5	211	*Pn3m*	97.6 ± 2.2
	34.2	220		
	32.1	221, 300		
MO/H_2O/cAMP (57.3:39.5:3.2 wt.%)	72.7	110		
	58.8	111		
	50.9	200		
	41.9	211	*Pn3m*	101.7 ± 1.8
	36.4	220		
	34.6	221, 300		
MO/D_2O/cAMP (58.4:38.8:2.8 wt.%)	70.1	110		
	57.6	111		
	50.3	200		
	40.4	211	*Pn3m*	98.6 ± 2.4
	35.4	220		
	33.5	221, 300		
MO/H_2O/dbcAMP (58.4:38.4:3.2 wt.%)	64.1	211		
	57.5	220		
	43.5	321		
	40.4	400	*Ia3d*	160.5 ± 1.1
	36.2	420		
	34.4	332		
MO/D_2O/dbcAMP (56.8:40.0:3.2 wt.%)	65.5	211		
	57.1	220		
	42.8	321	*Ia3d*	161.1 ± 1.8
	40.0	400		
	35.7	420		
	34.5	332		

[a] Values are given ± S.E. of the best linear fit ($r \geq 0.9980$) of the experimental points to the equation $d_{hkl} = a_o/(h^2 + k^2 + l^2)^{1/2}$.

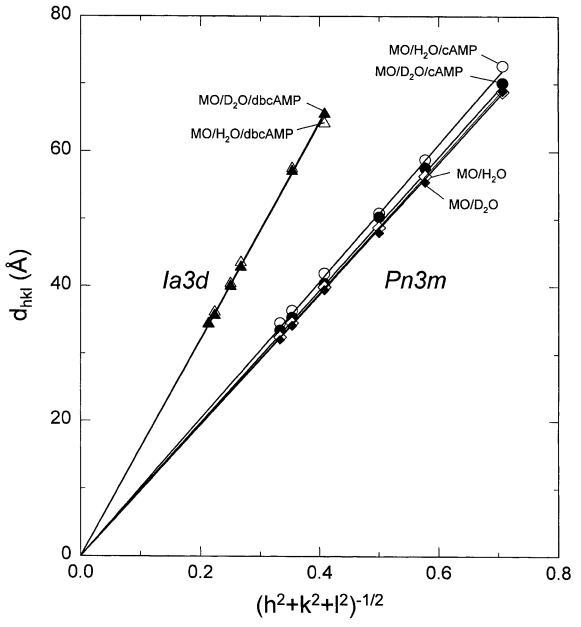

Fig. 3. Plot of d_{hkl} vs. $(h^2+k^2+l^2)^{-1/2}$ of the reflections obtained for the dbcAMP-containing samples (cubic phases of space group *Ia3d*), and for the reference and cAMP-containing systems (cubic phases of space group *Pn3m*). The sample compositions and calculated lattice constants are presented in Table 1.

h, k and l are the Miller indices. For the correct choice of space group, this plot gives a straight line passing through the origin and having a slope of the unit cell axis (a_o).

For the pseudobinary and cAMP-containing pseudoternary phases, six separate reflections are observed, which could be indexed according to the primitive cubic lattice of space group *Pn3m*. The fit of the cubic lattice relationship, given above in the experimental results of the MO sample containing 39 wt.% of H_2O (Fig. 3), resulted in an a_o value of 97.0 ± 0.9 Å (value $\pm$ S.E. of the linear fit; correlation coefficient $r = 0.9998$), which is only slightly decreased when compared to the pure 1-monooleoylglycerol/water system [7,8]. Although D_2O and cAMP leave the diffraction pattern of the *Pn3m* cubic phase practically unaltered, the pseudoternary sample containing the highest amounts of H_2O (39.5 wt.%) and cAMP (3.2 wt.%) is characterized by slightly increased a_o (approx. 102 Å). However, since this lattice parameter is obtained from a single sample measurement, the increased swelling of the $MO/H_2O/cAMP$ phase should be considered with some caution.

As distinct from the cAMP-containing cubic phases, for the pseudoternary systems with entrapped dbcAMP, six Bragg reflections could be assigned to the body-centered cubic lattice of space group *Ia3d*. The d_{hkl} vs. $(h^2+k^2+l^2)^{-1/2}$ plots shown in Fig. 3 give the a_o values of approximately 160 Å for the H_2O-and D_2O-containing systems. This result is quite surprising since, using the same commercial preparation of MO, we have demonstrated that a lattice parameter of approximately 140 Å is reached at the maximum swelling (< 34 wt.% water) of the pseudobinary *Ia3d* phase [9].

Thus, our SAXD data indicate that the entrapment of approximately 3 wt.% dbcAMP into the *Pn3m* phase of MO leads to the intercubic *Pn3m* → *Ia3d* transition. This experimental fact deserves more detailed consideration, and we will do that by analyzing the local geometrical parameters of a MO pseudomolecule (an amphiphilic molecule with the average geometrical parameters of the molecular MO mix) in the phases under discussion.

It has been demonstrated by Israelachvili et al. [23] that the lipid geometry in the self-assembled structures is most conveniently characterized by the dimensionless lipid shape parameter $V/(Al)$, which relates the molecular volume (V) to the lipid head-group area (A) and lipid length (l; normal to the interface). For the reversed liquid–crystalline phases, the shape parameter exceeds unity, and it generally varies between 1.05 and 1.5 for the cubic phases [23,24]. However, to express the shape parameter in terms of a_o or phase composition, the geometrical and topological features of the reversed bicontinuous cubic phases must be taken into account.

As mentioned in the introduction, it is believed that the 'gyroid'- (G) and 'diamond'-type (D) infinite periodic minimal surfaces (IPMS) (Fig. 2) afford structural models of the *Ia3d* and *Pn3m* cubic phases of aqueous MO, respectively. These two IPMS can be distinguished by their topology,

which characterizes the connectivity of the channel network of the bicontinuous morphology. The topology of the bilayer, conventionally parameterized by the Euler–Poincaré characteristic (χ) per unit cell of the underlying IPMS, is linked to the surface-averaged Gaussian curvature [$\langle K \rangle$] of IPMS by the following equation:

$$\langle K \rangle A_{uc} = 2\pi\chi, \quad (1)$$

where A_{uc} is the IPMS area per unit cell. The value of χ has been calculated by a number of authors and equals -8 for the G- and -2 for the D-type IPMS.

For the present purposes, one more global parameter of the IPMS form is important. This is a dimensionless constant, known as the 'homogeneity index' (H), which links A_{uc}, χ and a_o:

$$H \equiv (A_{uc})^{3/2} / \left[(-2\pi\chi)^{1/2} a_o^3 \right]. \quad (2)$$

The value of H also depends on the IPMS and is 0.7665 and 0.7498 for the G- and D-type minimal surfaces, respectively.

Let us assume that the head-groups of MO pseudomolecules lie on the plane which is moved away from the underlying IPMS by a constant distance l, i.e. a polar/apolar interface is parallel to the IPMS. In such a situation, according to differential geometry, the surface-averaged head-group area of the pseudomolecule ($\langle A \rangle$) is given by Eq. (3):

$$\langle A \rangle = \langle A_o \rangle (1 + \langle K \rangle l^2), \quad (3)$$

where $\langle A_o \rangle$ is the surface-averaged area per pseudomolecule at the mid-surface of bilayer. Further, the parallel surface model gives the averaged volume of MO pseudomolecule [$\langle V \rangle$]:

$$\langle V \rangle = \langle A_o \rangle l [1 + (\langle K \rangle l^2 / 3)]. \quad (4)$$

A combination of Eqs. (1)–(4) enables one to express the surface-averaged shape parameter by the following equation:

$$\langle V \rangle / [\langle A \rangle l] = \left[1 + (2\pi\chi l^2 / 3\sigma a_o^2) \right] / \left[1 + (2\pi\chi l^2 / \sigma a_o^2) \right], \quad (5)$$

where $\sigma = (-2\pi\chi H^2)^{1/3}$.

On the other hand, the same model of parallel surfaces gives the relation between the volume fraction of bilayer (Φ_L) and shape parameter (for convenience, $\langle V \rangle / \langle A \rangle l$ is denoted by s in the equation) [24]:

$$\Phi_L = 4 \times 3^{1/2} H s \left[(s-1)/(3s-1)^3 \right]^{1/2}. \quad (6)$$

Thus, once the value of l is chosen or known, Eqs. (5) and (6) provide a means of estimating $\langle V \rangle / \langle A \rangle l$ and, thence, Φ_L using the experimental parameter a_o. Based on our earlier investigation of the swelling behavior of MO cubic phases (the same commercial preparation of MO has been studied over the H_2O content interval of 13–40 wt.%) [9], we performed these calculations by setting $l = 17.2$ Å. Fig. 4 presents the results together with the theoretical curves [Eq. (6)] for the bicontinuous mesophases of *Ia3d* and *Pn3m* symmetries.

Although the errors in the estimated values of $\langle V \rangle / \langle A \rangle l$ [determined by the SE values of a_o in Eq. (5)] and Φ_L [determined by the consecutive application of Eqs. (5) and (6)] are rather high (particularly for the MO/D_2O and cAMP-containing systems), some useful conclusions can be drawn from Fig. 4.

First, for the *Pn3m* cubic phases, a simultaneous decrease in the shape and composition parameters according to the order MO/H_2O > MO/D_2O > MO/D_2O/cAMP > MO/H_2O/cAMP reflects surprisingly well a decrease in the MO content in these samples (Table 1). In other words, this result is consistent with the conventional viewpoint that the swelling with water of the reversed bicontinuous cubic phases necessarily means a reduction in the wedge-shape of lipid molecules.

Second, since it is well known that the *Pn3m* phase of 1-monooleoylglycerol [6–8] and MO preparation [9] transforms to the *Ia3d* phase with increasing Φ_L (decreasing hydration), our SAXD data (Table 1) and Fig. 4 reveal that dbcAMP stabilizes the *Ia3d* phase at unusually low values

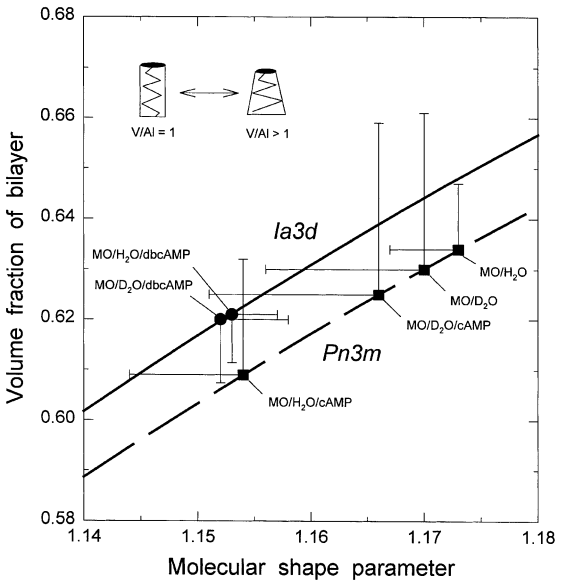

Fig. 4. Plot of 'volume fraction of bilayer' (Φ_L) vs. 'molecular shape parameter' [$\langle V\rangle/(\langle A\rangle l)$ or s] of the data points calculated [Eqs. (5) and (6)] for the dbcAMP-containing samples (filled circles), and for the reference and cAMP-containing systems (filled squares), together with the completely theoretical [Eq. (6)] curves for the *Ia3d* (full curve) and *Pn3m* (long-dashed curve) cubic structures. The lattice constants $\pm$S.E., used in the calculations of the data points and their errors, as well as sample compositions are presented in Table 1. Inset schematically illustrates the relation between the molecular shape and shape parameter.

of Φ_L and $\langle V\rangle/\langle A\rangle l$. In contrast, more polar nucleotide, cAMP, does not exhibit this property. Therefore, it might be speculated that the effect is determined by some type of interaction between the MO bilayer and dbcAMP.

Here, we recall that the above analysis is based on the assumption that the polar/apolar interface is parallel to the underlying IPMS. The alternative is to represent the interface as a surface of constant mean curvature. However, the visualization and mathematics of the latter model become somewhat more complicated (see, e.g. Anderson et al. [25] and Grosse-Brauckmann [26]). Therefore, considering the main objective of the present work, we will not pursue the theoretical modeling of our systems. Rather, to check the validity of the above hypothesis, we extended the investigation of the cAMP- and dbcAMP-containing systems through the use of Raman spectroscopy. It is well-known that this technique provides valuable information on the molecular interactions and dynamics.

3.2. Interactions of cAMP and dbcAMP with MO bilayer as monitored by Raman spectroscopy

Using vibrational spectroscopy, the substance–lipid interactions are generally analyzed by determining the way in which each component influences the vibrational modes of the other. In this part of the paper, we will deal with the Raman scattering characteristics of cAMP and dbcAMP first.

3.2.1. Vibrational modes of cAMP and its dibutyryl analogue

Fig. 5a and Fig. 6a present Raman spectra of the MO/H_2O/cAMP and MO/H_2O/dbcAMP cubic phases over the wavenumber range of 600–1800 cm^{-1}. As could be expected under these sample compositions, only a few bands in the spectra of the pseudoternary phases can be associated with the cyclic nucleotides. Thus, when compared to the Raman features of the *Pn3m* cubic phase of aqueous MO (Fig. 5b), the spectrum of the cAMP-containing sample (Fig. 5a) exhibits two additional bands of low intensity at approximately 1338 (shoulder) and 1580 cm^{-1}. Similarly, for the dbcAMP-containing phase, only three features at 1168, 1356 and 1587 cm^{-1} can be assigned to the vibrational modes of dbcAMP (see Fig. 6a,b).

As opposed to the observed spectra of the pseudoternary phases, the digital difference spectra (spectrum of the pseudoternary sample minus spectrum of the reference pseudobinary system, satisfying a criterion of zero intensity of the 1656-cm^{-1} MO peak) shown by traces (a)–(b) in Figs. 5 and 6 reveal a number of peaks, most of which agree closely with the spectral features of cAMP and dbcAMP in H_2O (Fig. 5c and Fig. 6c, respectively). Here, attention must be drawn to the fact that reference spectra (b) in the figures pertain to the same pseudobinary cubic phase of *Pn3m* symmetry, whereas, as shown above, the db-

cAMP-containing phase is characterized by the space group symmetry *Ia3d*. However, trace (d) in Fig. 6, which is achieved by subtracting reference spectrum (b) from the spectrum (not shown) of the MO/H_2O sample containing 26 wt.% H_2O (the *Ia3d* cubic phase is formed at this composition [9]), clearly demonstrates that spectrum (a)–(b) in Fig. 6 represents predominantly features of the entrapped dbcAMP. Given this result, we now may pursue a comparison analysis of the corresponding traces (a)–(b) and (c) in more detail. For this purpose, Table 2 summarizes the band frequencies and assignments for the cyclic nucleotides in H_2O and D_2O over the wavenumber range of 600–3050 cm^{-1}. However, since the spectral region 1800–3050 cm^{-1} did not reveal any reliable differences in the Raman features of the entrapped and solubilized nucleotides, this frequency range was omitted from the following discussion.

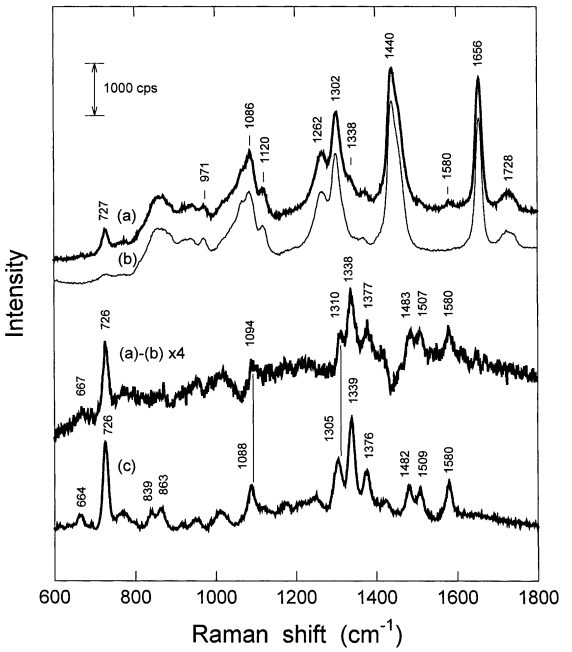

Fig. 5. Raman spectra of: (a) the cubic $MO/H_2O/cAMP$ phase of 57.3:39.5:3.2 wt.% composition; (b) the cubic MO/H_2O phase of 61:39 wt.% composition; and (c) the 0.6 M cAMP solution in H_2O. Excitation, 514.5 nm. Integration time, 4 s. Three scans were co-added for one spectrum. The digital difference spectrum (a)–(b) is also shown (spectrum of the cAMP-containing cubic phase minus spectrum of the cubic MO/H_2O phase, satisfying a criterion of zero intensity of the 1656-cm^{-1} MO peak).

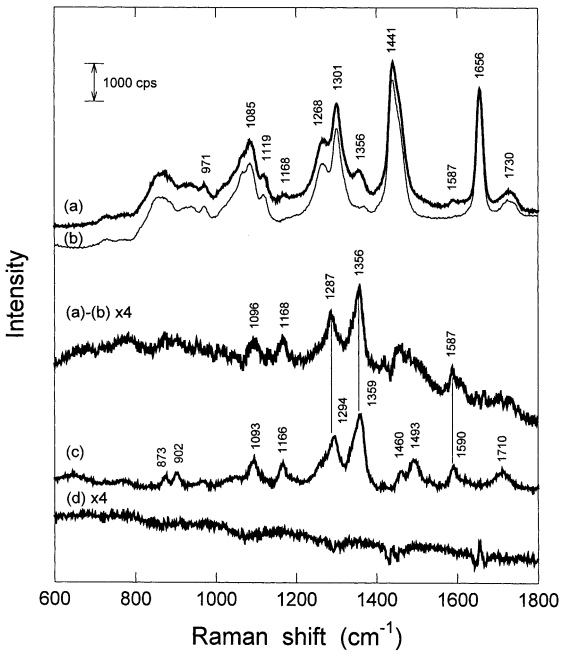

Fig. 6. Raman spectra of: (a) the cubic $MO/H_2O/dbcAMP$ phase of 58.4:38.4:3.2 wt.% composition; (b) the cubic MO/H_2O phase of 61:39 wt.% composition; and (c) the 0.3 M dbcAMP solution in H_2O. Excitation, 514.5 nm. Integration time, 4 s. Three scans were co-added for one spectrum (a) or (b), whereas four scans were co-added for one spectrum (c). Digital difference spectrum (a)–(b) is also shown (spectrum of the dbcAMP-containing cubic phase minus spectrum of the cubic MO/H_2O phase, satisfying a criterion of zero intensity of the 1656-cm^{-1} MO peak). Trace (d) demonstrates the digital difference spectrum, achieved by subtracting spectrum (b) from the spectrum (not shown) of the Ia3d cubic MO/H_2O phase of 74:26 wt.% composition.

When assigning vibrational modes, we refereed extensively to the earlier investigations of different nucleotides and their models [27–37]. Thus, it is well known that vibrations in adenine nucleotides are extensively coupled because of the lack of symmetry and large ring system consisting of the fused cycles of six-membered pyrimidine (Pyr) and five-membered imidazole (Im) (see Fig. 1). Nevertheless, the investigations performed with ^{15}N-, ^{13}C-, and D-labeled adenine rings, coupled with normal coordinate analysis have led to

Table 2
Raman peak-frequencies (cm^{-1}) and vibration assignments of the cAMP and dbcAMP solutions in H_2O and D_2O

cAMP[a]		dbcAMP[a]		Assignment[b]
H_2O	D_2O	H_2O	D_2O	
3007 w		3009 sh	3009 sh	ν(C–H) ring
2956 w, sh	2963 ?			ν(C–H)
		2944 m	2944 m	ν(C–H)
2910 m	2911 m	2913 m	2914 m	ν(C–H)
		2880 m	2881 m	ν(C–H)
		1710 m	1693 m	ν(C=O)
	1621 vw	1622 w, sh		Pyr + δ(NH_2)
1580 s	1578 s	1590 s	1590 s	Pyr
1509 s	1518 m	1493 s, br	1507 s	Im
1482 s	1483 s	1493 s, br	1478 s	Pyr + Im
		1460 m	1465 sh	δ(CH_2)
1425 vw	1427 vw	1416 vw	1423 sh	Im
1376 s	1380 m		1391 s	Pyr + Im
1339 vs	1342 vs	1359 vs	1345 vs	Pyr
1305 s	1305 vs	1294 vs	1284 vs	Pyr and/or Pyr + Im
1248 w	1247 w, sh	1262 sh	1220 w, sh	$\nu_{as}(PO_2^-)$; Pyr + Im
1175 vw	1183 s	1166 s	1174 s	Im + ν(N9–C1′)
1088 s	1090 s	1093 s	1092 s	$\nu_s(PO_2^-)$
1011 m	1043 w	1050 w, sh	1043 w	ν(C–O; C–C) ribose; Pyr + Im
952 w		967 w	961 vw	ν(C–O) ribose
863 m	862 s	902 m	903 m	Im
769 w	772 m	767 vw	771 w	$\nu_s(PO_2^*)$
726 vs	718 vs	725 ?		Pyr + Im
664 w	664 m	645 m	655 vw	Ribose–phosphate moiety

[a] *Abbreviations:* ν, stretching; δ, deformation; s, strong; vs, very strong; w, weak; vw, very weak; m, middle; sh, shoulder; br, broad; Pyr, vibration of pyrimidine ring; Im, vibration of imidazole ring; O*, ester oxygen atom.
[b] Assignments are based on refs. [27–37].

the assignment of certain vibrations concentrated on the motions of particular molecular group or one of the rings. Moreover, it has been demonstrated that a number of those modes are useful for the identification of the intermolecular interaction sites. For example, as in the case of other adenine-containing substances [29,31,36], the band for aqueous cAMP at 1509 cm^{-1} (see Fig. 5c and Table 2) is associated with the motion of Im ring and serves as a marker band of the N7-site. As shown in Table 2, for cAMP in D_2O, the N7-site mode undergoes the frequency upshift by 9 cm^{-1}. The corresponding bands for dbcAMP in H_2O and D_2O are observed at approximately 1493 and 1507 cm^{-1} (Fig. 6c and Table 2). However, as evident from Fig. 5, the entrapment of cAMP in the cubic phase of MO leaves the characteristics of this marker mode practically unaltered, and the same is true for the majority of the cAMP ring modes, with one exception. In the cAMP-containing phase, the 'Pyr and/or Pyr + Im' vibration band is upshifted by 5 cm^{-1} and appears at 1310 cm^{-1} (Fig. 5). At this point, we note the first difference in the effects of entrapment of these two cyclic nucleotides in the cubic phases. Thus, as opposed to the ring modes of cAMP, the 1294-, 1359- and 1590-cm^{-1} ring features in the aqueous dbcAMP (Fig. 6c) undergo a significant downward shift by 7, 3 and 3 cm^{-1}, respectively, upon the incorporation of this cAMP analogue in the MO phase. Interestingly, the above-mentioned modes for dbcAMP are basically due to the Pyr ring (Table 2).

Another important difference between the ef-

fects of phase matrix on the Raman features of cAMP and dbcAMP comes from the analysis of the phosphate group modes.

It is well known that the presence of two pairs of non-equivalent oxygen atoms in the phosphate group, ester oxygen atoms (denoted as O*; see Fig. 1) and anionic oxygen atoms (denoted as O^-), results in the appearance of two sets of stretching vibrations: (i) the symmetric $\nu_s(PO_2^*)$ and asymmetric $\nu_{as}(PO_2^*)$ stretching motions at approximately 750 and 820 cm^{-1}; and (ii) the corresponding $\nu_s(PO_2^-)$ and $\nu_{as}(PO_2^-)$ vibrations at approximately 1090 and 1220 cm^{-1} [30,32–35]. However, the ν_s bands always exhibit considerably higher Raman intensity compared to the ν_{as} features [32,35]. Besides, the positions of the $\nu_s(PO_2^*)$ and $\nu_{as}(PO_2^*)$ modes are indicators of the conformations in the C–O*–P–O*–C segment [34], whereas the peak-frequencies of the PO_2^- stretching vibrations are sensitive to the interactions of this group with water molecules [30,34]. Thus, the hydrogen bonding $PO^{-\bullet\bullet\bullet}HOH$ decreases the frequency of both PO_2^- stretching modes, and yet the effect is more pronounced for the $\nu_{as}(PO_2^-)$ mode.

As can be seen from Table 2, the $\nu_s(PO_2^-)$ mode for the cAMP solution in H_2O is located at 1088 cm^{-1}. For the dbcAMP solution, this feature is slightly upshifted and centered at 1093 cm^{-1}. The bands of low intensity at 769 cm^{-1} (cAMP/H_2O) and 767 cm^{-1} (dbcAMP/H_2O) can be assigned to the $\nu_s(PO_2^*)$ mode (Table 2). At the same time, as one would expect, the ν_{as} vibrations are not clearly defined in the spectra.

Inspection of traces (a)–(b) and (c) in Fig. 5 shows that, in the cAMP-containing cubic phase, the band arising from the symmetric vibration of PO_2^- is shifted to the higher frequency region by approximately 6 cm^{-1} (4 cm^{-1} in the D_2O-based phase; data not shown) as compared to the 1088-cm^{-1} peak of this feature in the aqueous nucleotide solution. Since the symmetric mode is less sensitive to the degree of hydration than the asymmetric one [30,34], the shift observed should be regarded as quite significant. Similarly, comparison of traces (a)–(b) and (c) for dbcAMP (Fig. 6) also reveals the upward shift of the $\nu_s(PO_2^-)$ mode in the cubic phase; however, the effect does not exceed 3 cm^{-1} (2 cm^{-1} in the D_2O-based cubic phase; data not shown). As noted above, the $\nu_s(PO_2^-)$ band shifts to the lower frequencies as the hydration of PO_2^- increases. Therefore, the upward shift of the band can be related to the decreased hydration or weaker H-bonding of the PO_2^- group in the MO cubic phase.

We now are in a position to make some preliminary conclusions from the above Raman scattering experiments. First, there are grounds to believe that, as distinct from the adenine ring of cAMP, the butyryladenine group of dbcAMP partitions, to some extent, into the MO bilayer of the cubic phase. Secondly, it is conceivable that this interaction furnishes a higher degree of hydration or stronger H-bonding of the PO_2^- group of dbcAMP compared to that of cAMP. Two effects of the lipidic matrix on the Raman characteristics of the nucleotides support our conclusions: (i) the adenine ring modes for cAMP and dbcAMP shift to the opposite directions; and (ii) the upward shift of the $\nu_s(PO_2^-)$ mode is significantly less pronounced in the case of dbcAMP. The following section is intended to provide additional experimental proof of these conclusions.

3.2.2. Raman features of MO pseudomolecule

The characteristic property of the Raman spectra of lipids is that they predominantly contain bands arising from vibrations of the hydrocarbon chains. These Raman features can be observed over a wide range of wavenumbers spanning from 10 to over 3000 cm^{-1} [27,38,39]. However, as one might immediately anticipate from the composition of the pseudoternary phases, there is very little hope for finding the cAMP- or dbcAMP-induced changes in the spectral characteristics of MO. Nevertheless, in our opinion, we have succeeded in revealing one Raman feature of MO, namely the methylene twisting band, $\delta_t(CH_2)$, at approximately 1300 cm^{-1}, which undergoes a modest change in the dbcAMP-containing pseudoternary phase.

The effect was established by the analysis of the observed and digital difference spectra. However, here, the difference spectra were acquired by the subtraction of the nucleotide solution spectrum from the observed spectrum of the cor-

responding pseudoternary phase. The interactive subtraction was performed to satisfy the criterion of zero intensity of the following peaks: 718-cm^{-1} for cAMP in D_2O; 726-cm^{-1} for cAMP in H_2O; and 1590-cm^{-1} for dbcAMP.

Table 3 presents the peak-frequencies and full-widths at half-height (FWHH) of the $\delta_t(CH_2)$ mode, which are obtained upon the deconvolution of the reference (pseudobinary samples) and difference spectra. It is quite evident from the data in Table 3 that the position of the peak is practically independent of the cubic phase composition, but the FWHH parameter somewhat increases in the dbcAMP-containing phases. According to the investigations by Larsson and Rand [40], the formation of gauche conformers in the hydrocarbon chain of lipids causes broadening of the methylene twisting band. This interpretation is supported by our earlier Raman studies of MO [41]. Thus, we have demonstrated that the FWHH value increases in conformity of the order: solid MO < *Pn3m* MO/H_2O phase < melted MO (the FWHH values are not provided, since the composition of MO preparation used in the present study is different).

Considering the above results, we could conclude that the presence of dbcAMP in the cubic phase increases the conformational disorder along the acyl chain of MO. However, although this conclusion is consistent at first glance with the above hypothesis that dbcAMP partitions into the MO bilayer, we must treat the observed effect with some caution. Thus, it is well known that, when compared to the $\delta_t(CH_2)$ mode, the C–H stretching vibrations (2800–3000 cm^{-1}) are more sensitive to the conformational state and mobility of the hydrocarbon chains of lipids [40–42]. However, we found no reliable differences in the Raman features of the reference and difference spectra over the wavenumber range from 2800 to 3100 cm^{-1}.

Table 3
Raman peak-frequencies and full-widths at half-height (FWHH) of the MO methylene twisting, $\delta_t(CH_2)$, band in the cubic phases

Cubic phase sample	$\delta_t(CH_2)$ (cm^{-1})[a]	FWHH (cm^{-1})[b]
MO/H_2O (61:39 wt.%)	1302	27.5
MO/H_2O/cAMP (57.3:39.5:3.2 wt.%)	1302	27.9
MO/H_2O/dbcAMP (58.4:38.4:3.2 wt.%)	1302	30.9
MO/D_2O (60.9:39.1 wt.%)	1303	29.9
MO/D_2O/cAMP (58.4:38.8:2.8 wt.%)	1304	30.4
MO/D_2O/dbcAMP (56.8:40.0:3.2 wt.%)	1302	33.4

[a] Uncertainty in peak frequencies is not higher than ± 1 cm^{-1}.
[b] Uncertainty in FWHH is not higher than ± 1.5 cm^{-1}.

4. Conclusions

Based on the small-angle X-ray diffraction and Raman scattering studies of the cAMP- and dbcAMP-containing bicontinuous cubic phases of aqueous MO, we found that, as opposed to cAMP, dbcAMP is capable of partitioning into the MO bilayer. In the SAXD experiments, the interaction of dbcAMP with MO bilayer was reflected by the nucleotide-induced intercubic *Pn3m* → *Ia3d* transition. Different effects of the cubic phase matrix on the Raman shifts of the adenine and phosphate vibration modes provided additional proof of the partitioning of dbcAMP into the MO bilayer. Moreover, the Raman scattering measurements suggested that this cAMP analogue inserts into the bilayer through the butyryladenine group, to say the least. However, since the flat shape and aromaticity of dbcAMP's adenine should limit deeper insertion into the hydrophobic interior of bilayer [for more thorough analysis and discussion of this general problem, see, e.g. Uau et al. [43] and White and Wimley [44]], the interaction positions dbcAMP preferentially at the polar/apolar interface. Because of such interfacial localization, the degree of hydration or the H-bonding capacity of the dbcAMP's phosphate group decreases only slightly, whereas the effect is more pronounced for the phosphate group of the entrapped cAMP. Although we do not have an adequate explanation for the latter result, it also demonstrates a different environment of these cyclic nucleotides in the cubic phases of MO. Clearly, to gain a better insight into the molecular and supramolecular features of the MO/H_2O/cAMP and MO/H_2O/dbcAMP systems,

the determination of the phase diagrams is required. Experiments along these lines are in progress. On the other hand, the bicontinuous cubic phases containing zwitter-ionic phospholipids should be applied for revealing possible effects of the electrostatic interaction between phospholipid and cAMP on the physicochemical properties of bilayer.

Acknowledgements

This work was supported by the Royal Swedish Academy of Sciences.

References

[1] E.W. Sutherland, T.W. Rall, J. Biol. Chem. 232 (1958) 1077.
[2] G.A. Morrill, K. Doi, J. Erlichman, A.B. Kostellow, Biochim. Biophys. Acta 1158 (1993) 146.
[3] Y.-M. Li, M. Wei, Y.-F. Zhao, J.-Y. Yu, Q. Zhou, Spectrosc. Lett. 32 (1999) 197.
[4] T. Posternak, E.W. Sutherland, W.F. Henion, Biochim. Biophys. Acta 65 (1962) 558.
[5] T. Landh, FEBS Lett. 369 (1995) 13.
[6] S.T. Hyde, S. Andersson, B. Ericsson, K. Larsson, Z. Krystallogr. 168 (1984) 213.
[7] J. Briggs, H. Chung, M. Caffrey, J. Phys. II France 6 (1996) 723.
[8] H. Qiu, M. Caffrey, Biomaterials 21 (2000) 223.
[9] J. Barauskas, V. Razumas, T. Nylander, Chem. Phys. Lipids 97 (1999) 167.
[10] G. Lindblom, K. Larsson, L. Johansson, K. Fontell, S. Forsen, J. Am. Chem. Soc. 101 (1979) 5465.
[11] S. Andersson, S.T. Hyde, K. Larsson, S. Lidin, Chem. Rev. 88 (1988) 221.
[12] K. Larsson, J. Phys. Chem. 93 (1989) 7304.
[13] J.M. Seddon, R.H. Templer, Phil. Trans. R. Soc. Lond. A 344 (1993) 377.
[14] V. Luzzati, H. Delacroix, A. Gulik, T. Gulik-Krzywicki, P. Mariani, R. Vargas, Curr. Top. Membr. 44 (1997) 3.
[15] S. Engström, T.P. Norden, H. Nyquist, Eur. J. Pharm. Sci. 8 (1999) 243.
[16] S. Vauthey, P. Visani, Ph. Frossard, N. Garti, M.E. Leser, H.J. Watzke, J. Disp. Sci. Technol. 21 (2000) 263.
[17] E.M. Landau, J.P. Rosenbusch, Proc. Natl. Acad. Sci. USA 93 (1996) 14532.
[18] G. Rummel, A. Hardmeyer, C. Widmer et al., J. Struct. Biol. 121 (1998) 82.
[19] V. Razumas, K. Larsson, Y. Miezis, T. Nylander, J. Phys. Chem. 100 (1996) 11766.
[20] F. Caboi, T. Nylander, V. Razumas, Z. Talaikyte, M. Monduzzi, K. Larsson, Langmuir 13 (1997) 5476.
[21] V. Razumas, J. Kanapieniene, T. Nylander, S. Engström, K. Larsson, Anal. Chim. Acta 289 (1994) 155.
[22] T. Nylander, C. Mattisson, V. Razumas, Y. Miezis, B. Håkansson, Colloid Surf A: Physicochem. Eng. Aspects 114 (1996) 311.
[23] J.N. Israelachvili, D.J. Mitchell, B.W. Ninham, J. Chem. Soc. Faraday Trans. 272 (1976) 1525.
[24] S. Hyde, S. Andersson, K. Larsson et al., The Language of Shape. The Role of Curvature in Condensed Matter: Physics, Chemistry and Biology, Elsevier, Amsterdam, 1997.
[25] D.M. Anderson, H.T. Davis, L.E. Scriven, J.C.C. Nitsche, Adv. Chem. Phys. 77 (1990) 337.
[26] K. Grosse-Brauckmann, J. Colloid Interface Sci. 187 (1997) 418.
[27] P.R. Carey, Biochemical Applications of Raman and Resonance Raman Spectroscopies, Academic Press, New York, 1982.
[28] M. Tsuboi, Y. Nishimura, A.Y. Hirakawa, W. Peticolas, in: T.G. Spiro (Ed.), Biological Applications of Raman Spectroscopy 2, Wiley, New York, 1987, p. 109.
[29] J. Wiorkiewicz-Kuczera, M. Karplus, J. Am. Chem. Soc. 112 (1990) 5324.
[30] W. Pohle, M. Bohl, H. Böhlig, J. Mol. Struct. 242 (1990) 333.
[31] A. Toyama, N. Hanada, Y. Abe, H. Takeuchi, I. Harada, J. Raman Spectrosc. 25 (1994) 623.
[32] Y. Guan, C.J. Wurrey, G.J. Thomas, Jr., Biophys. J. 66 (1994) 225.
[33] Y. Guan, G.S.-C. Choy, R. Glaser, G.J. Thomas, Jr., J. Phys. Chem. 99 (1995) 12054.
[34] Y. Guan, G.J. Thomas, Jr., J. Mol. Struct. 379 (1996) 31.
[35] J. Florian, V. Baumruk, M. Štrajbl, L. Bednarova, J. Štepanek, J. Phys. Chem. 100 (1996) 1559.
[36] J. Štepanek, J. Kowalewski, J. Lang, P. Mojzeš, J. Biol. Inorg. Chem. 3 (1998) 543.
[37] W. Pohle, C. Selle, H. Fritzsche, H. Binder, Biospectroscopy 4 (1998) 267.
[38] I.W. Levin, in: R.J.H. Clark, R.E. Hester (Eds.), Advances in Infrared and Raman spectroscopy 11, Wiley, Heyden, 1984, p. 1.
[39] D. Chapman, F.M. Goni, in: F.D. Gunstone, J.L. Harwood, F.B. Padley (Eds.), The Handbook of Lipids, 2nd ed. Chapman and Hall, London, 1994, p. 505.
[40] K. Larsson, R.P. Rand, Biochim. Biophys. Acta 326 (1973) 245.
[41] V. Razumas, Z. Talaikyte, J. Barauskas, K. Larsson, Y. Miezis, T. Nylander, Chem. Phys. Lipids 84 (1996) 123.
[42] R. Mendelsohn, Biochim. Biophys. Acta 290 (1972) 15.
[43] W.-M. Yau, W.C. Wimley, K. Gawrisch, S.H. White, Biochemistry 37 (1998) 14713.
[44] S.H. White, W.C. Wimley, Annu. Rev. Biophys. Biomol. Struct. 28 (1999) 319.